Lattice Boltzmann Method With Ghost Flow In Curve Boundary For Simulation Aerodynamic Force Around Airfoil

Hamed Saffarzadeh
PhD student, Ferdowsi university of Mashhad, Engineering Department
Hamed.saffarzadeh@gmail.com

Mohammad Hassan Djavareshkian
Professor, Ferdowsi university of Mashhad, Engineering Department
javareshkian@ferdowsi.um.ac.ir

Abstract

In this paper, a ghost flow in lattice Boltzmann method is developed to simulate aerodynamic flow around on airfoil for curved boundaries. A bilinear interpolation is developed to simulate for two-dimensional fluid flow around airfoil (NACA 0012). The results of the presented method are compared to those available in the literature from conventional numerical methods, and excellent agreement is observed. Curved boundary treatments have been suggested as a means of improving the accuracy of the stair-shaped approximation conventionally used in LBM simulations and this technic can capture the details of flow more accurately and more stable than the other methods, in low- Reynolds-number flow. This simulation is presented to solve fluid dynamics based on the theory molecule kinetics; an extended Lattice Boltzmann equation is put forward to solve force in Reynolds number range that be applicative for Micro-Air-Vehicles (MAVs).

Key words: lattice Boltzmann, ghost fluid method, Curved boundary, Aerodynamic

1. Introduction

The lattice Boltzmann methods[1] are a relatively recent approach to computational fluid dynamics (CFD), which has been proven to be successful in a broad range of applications, low Reynolds range[2], to multiphase and free-surface flows [3], as well as to non-Newtonian flows [4], fluid-structure interaction problems, porous media [5] and beyond. LBM has been extensively studied in last several decades and witnessed as capable like conventional methods for various fluid problems. LBM has its own procedure to solve fluid problems and aforementioned Boltzmann equation (LBE) used to solve fluid flow instead of Navier-Stokes equation (NSE)[6]. Likewise, all numerical method boundary conditions give meaningfulness, accuracy, and numerical stability to LBM simulations. Bounce-back boundary condition was proposed to simulate no-slip condition on solid surface. Curve boundary techniques have been investigated widely in order to the accuracy of stair shaped which is employed in traditional LB simulation. That those methods are based on interpolation method but apply different mesh structure to execute distribution function throughout computational domain, non-uniform and uniform respectively. Interpolation-based types are the most commonly employed method for simulating curved boundary problems in LBM because of their inherent reliability and paramount numerical accuracy. These problems in applying stream flow conditions on the

curved boundaries are encountered not only in conventional numerical methods such as finite element and finite difference schemes based on discretizing the Navier–Stokes equations but also in the lattice Boltzmann method (LBM) originated from Boltzmann equation and kinetic theory of gasses[7]. Based on this kinetic nature, LBM solves the lattice Boltzmann equation on the uniform Cartesian grid which makes it difficult to deal with aerodynamic conditions at the curved boundaries.

Despite all these difficulties, the LBM due to its noble features such as ease of programming, linear nature, ease of parallelization, and high accuracy, has become a powerful numerical tool for solving the fluid flow and heat transfer problems in complex geometries[2]. During the last decade, many researches tried to improve the ability of the LBM in dealing with the curved boundaries. As the first attempt, Filippova and Hanel [8], and later Mei et al.[9] improved the bounce-back idea for satisfying the no-slip condition at the curved boundaries. In another work, Bouzidi et al. [10] proposed a new boundary treatment in which the bounce-back scheme was combined with an interpolation method. Later, Guo et al. [11] proposed a none-equilibrium distribution extrapolation method for applying the no-slip condition at the curved boundaries.

Another efficient approach to simulate fluid flow with curved boundaries is the ghost fluid method (GFM). In the ghost fluid lattice Boltzmann method (GFLBM), unknown distribution functions at ghost points are decomposed into their equilibrium and none-equilibrium parts. To construct the equilibrium part, the value of macroscopic variables at the ghost points are extrapolated from the related image and boundary points. To obtain the value of macroscopic variables at image points, various interpolation technics are used. The model, presented here, is deferent from previous work, that solved fluid dynamics based on the theory molecule kinetics, an extended Lattice Boltzmann equation is put forward to solve force modeled in Reynolds number range and combined with ghost flow for curve boundary, which has not been done in recently researches.

Consequently, present study tries to simulate flow over airfoil shape (NACA 0012), airfoil in the low Reynolds numbers regime, with the aim of further analyze the capabilities of the Ghost fluid LB model. Although the mentioned method enhances significantly the curve geometrical flexibility of LBM, in general, will be increased the complexity of the method itself, partially losing some key advantages. Moreover, this computational efficiency is considerably lower than that of traditional LBM. To overcome this limitation, we recently proposed a new lattice Boltzmann approach (NLBM) based on the coupling between a uniform grid model with ghost fluid and a curve node, body-fitted grid model. The NLBM retains the outstanding advantages of traditional LBM while bringing the flexibility of a Curve node discretization technic. Results demonstrate that the new method is robust and efficient, for this reason, it can be regarded as a viable approach to fluid dynamic problems involving curved geometries. Flow around an airfoil is calculated using LBM on generalized coordinates.

2. Numerical methodology

2-1. Equations of lattice Boltzmann method

In this paper, a D2Q9 lattice model is selected. The grid together with the sets of velocities and weights form the lattice. The D2Q9 lattice is a common choice for problems in two dimensions. It reduces the two-dimensional velocity space to a set of nine velocities and shown in figure 1. The velocities coordinates are here expressed in lattice units.

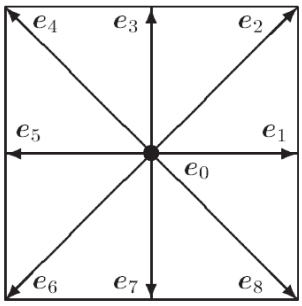

Figure 1. Schematic of the lattice links for the D2Q9 lattice Boltzmann model.

In this study, the velocity process is an incompressible flow regime. This method is governed by the following evolution equations with the single-relaxation-time approximation for the collision operator. Where τ_s and Δt_s being defined as momentum dimensionless relaxation time and the time step related to the normal node scheme, respectively. f is the density distribution functions along the i th direction, respectively, f_i^{eq} are the corresponding equilibrium distribution functions. i is associated with the discrete velocity $\vec{C}_i$ in the direction i

$$f_i(\mathrm{x}+\Delta t_s * \vec{C}_i . t + \Delta t_s) - f_i(x.t) = -\frac{\Delta t_s}{\tau_s}[f_i(x,t) - f_i^{eq}(x,t) \qquad (1)$$

Equilibrium distribution function f_i^{eq} (x, t) are calculated as follows:

$$f_i^{eq}(x,t) = w_i * \rho(x,t)\left[1 + \frac{c_i \cdot u(x,t)}{C_s^2} + \frac{(c_i \cdot u(x,t))^2}{2C_s^4} - \frac{(u(x,t))^2}{2C_s^2}\right] \qquad (2)$$

Where C_s is the lattice speed of sound (in this model $C_s \cong c/\sqrt{3}$), the parameters e_i are a set of weights normalized to unity that denotes the discrete velocity set, where i varies between 0 and 8 for D2Q9 model (Figure 1).

$$e_i = \begin{cases} (0,0) & \mathrm{i} = 0 \\ (\cos\left[(\mathrm{i}-1)\frac{\pi}{2}\right], \sin\left[(\mathrm{i}-1)\frac{\pi}{2}\right].\mathrm{C} & \mathrm{i} = 1,2,3,4 \\ (\cos\left[(\mathrm{i}-9)\frac{\pi}{4}\right], \sin\left[(\mathrm{i}-9)\frac{\pi}{4}\right].\sqrt{2}\mathrm{C} & \mathrm{i} = 5,6,7,8 \end{cases} \qquad (3)$$

ρ (x, t) and u (x, t) in Eq (2) are the macroscopic variables, namely fluid density and velocity, respectively. For an incompressible fluid flow, equation (1) reproduces the Navier-Stokes equations, with the kinematic viscosity being defined:

$$\upsilon = \frac{1}{3}(\tau_s - 0.5)C_s^2 * \Delta t_s \qquad (4)$$

Here, C =δt/δx in Eq (3) where δx is the lattice constant and δt is the time step, C is the lattice streaming speed which can take positive values to ensure that τ_s is greater than 0.5. w_i are the equilibrium distribution weighting factor for i th direction and can be given as follows:

$$w_i = \begin{cases} \frac{4}{9} & i = 0 \\ \frac{1}{9} & i = 1,3,5,7 \\ \frac{1}{36} & i = 2,4,6,8 \end{cases} \qquad (5)$$

The macroscopic aerodynamic quantities such as density, velocity, and pressure are obtained through the following equations:

$$\rho = \sum_{i=0}^{8} f_i \quad , \quad \rho u = \sum_{i=0}^{8} e_i f_i \quad , \; P = \rho C_s^2 \qquad (6)$$

The finite-volume lattice Boltzmann method adopted on the curve node grid is a cell vertex type method. The following equation applies at each node P of the grid:

$$f_i(P,t+\Delta t_u) = f_i(P,t) + \Delta t_u \sum_{k=0}^{\acute{k}} S_{ik} f_i(P_k,t) - \frac{\Delta t_u}{\Delta t_u} \sum_{k=0}^{\acute{k}} C_{ik}[f_i(P_k,t) - f_i^{eq}(P_k,t)] \quad (7)$$

Equation (7) derivation are provided in [12]. In equation (7) τ_u and Δt_u are the relaxation time and the time step, respectively related to the new scheme, k = 0 denotes the pivotal node P and the summations run over the nodes P_k connected to P; the quantities S_{ik} and C_{ik} represent the streaming and collisional matrices of the i-th population related to the k-th node, respectively; the equilibrium distribution function is defined by equation (2).

This method, equations (1) and (7) are solved consistently in time, with the exchange of information taking place at predefined interpolation nodes, which are placed over the overlapping grids region, in terms of both macroscopic variables and distribution functions. The following equations describe the post-collision for the normal node and curve boundary in ghost fluid nodes, respectively:

For Collision:

$$\tilde{f}_i^{N.eq}(x_i,t) - \tilde{f}_i^{C.eq}(x_i,t) = \tilde{f}_i^{noneq} * 2 * \frac{\tau_s - \Delta t_s}{\tau_s - \frac{\Delta t_s}{2}} \quad (8)$$

For Stream:

$$\tilde{f}_i^{C} - f_i^{N.eq} = \left[1 - \frac{\Delta t_s}{2*\tau_s}\right] \tilde{f}_i^{noneq} + \Delta t_u \Delta t_u \sum_{k=0}^{\acute{k}} S_{ik} \left\{ \grave{f}_{ik}^{eq} + \grave{f}_{ik}^{noneq} \right\} - \frac{\Delta t_u}{\Delta t_u} \sum_{k=0}^{\acute{k}} C_{ik} \grave{f}_{ik}^{noneq} \quad (9)$$

Where $\tilde{f}_i^{N.eq}$ and $\tilde{f}_i^{C.eq}$ refer to equilibrium distribution function for normal node and curve boundary respectively, and $\tilde{f}_i^{noneq}$ is the non-equilibrium distribution function. The quantities $\grave{f}_{ik}^{eq}$ *and* $\grave{f}_{ik}^{noneq}$ in the Eq (9) are defined as follows:

$$\grave{f}_{ik}^{eq} = f_{ik}^{Neq} \quad and \quad \grave{f}_{ik}^{Neq} = \left(1 - \frac{\Delta t_s}{2\tau_s}\right) * f_{ik}^{N.noneq}$$

Or (10)

$$\grave{f}_{ik}^{eq} = f_{ik}^{C.eq} \quad and \quad \grave{f}_{ik}^{noneq} = f_{ik}^{C.noneq}$$

Depending on whether the k-th node is on obstacle or not, respectively. The distribution functions $f_i^{C.eq}$ and $f_i^{C.noneq}$ of the right-hand side of equation (8) and $f_i^{N.eq}$ and $f_i^{n.noneq}$ of the right-hand side of equation (9) are evaluated by interpolation for curve boundary procedure.

2.2 Boundary treatment with the ghost fluid approach

In the present work, ghost fluid lattice Boltzmann formulation is developed to simulate boundary conditions on curved boundaries. The presented method can be described as described below. At first step is to find the ghost points (GP). As can be seen from Figure 2, nodes located inside the solid domain have at least one common link with the fluid nodes are considered as ghost points. Then must to find related image points (IPs) of ghost points determined in first

step. An (IP) is assumed to be on the normal line from the GP to the boundary, in such a way that the intersection point of the normal line with the boundary (BI) is at the halfway.

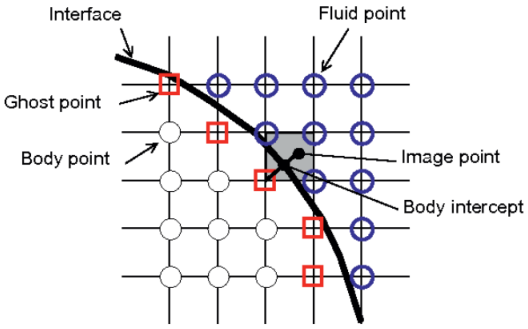

Figure 2. Schematic of the image point (IP), ghost point (GP), and boundary interface node (BI) as well as depiction of different situations encountered for interpolating the macroscopic variables at an image point.

After determining the image points, the main flow variables at IPs are interpolated using the information available from the neighboring fluid nodes. In this study, following the work of Tiwari and Vanka [17], for hydrodynamic curved boundaries, a bilinear interpolation method is used to estimate the value of general variables at IPs as described by Eq. (11):

$$\varphi = ax + by + cxy + d \tag{11}$$

Where φ denotes the value of general macroscopic variables such as density and velocity. In bilinear interpolation method, there are four unknown coefficients, namely, a, b, c, and d. Thus, four equations are needed to find these unknowns. For this purpose, values of x, y, and u corresponding to fluid neighboring points (NPs) were inserted into the Eq. (11) and then unknown coefficients are obtained. After calculating the coefficients, the values x and y of an image point is inserted into Eq. (11) to obtain the value of general variable (u).
For the former case, following the work of Tiwari and Vanka[13], these points can be replaced by the corresponding boundary intercept points. Also pointed out in their paper, there are some particular cases in which at least one of the NPs of an image point is not located in the fluid domain. To estimate velocity at an IP in the case of constant velocity boundary conditions, whenever one of the NPs is not interior, it is replaced by the boundary point halfway on the normal line drawn between the GP and the corresponding IP. Then, four equations are used to obtain the coefficients. These equations can be written in a generic form as:

$$\alpha(\alpha_i x_i + (1-\alpha_i)\acute{x_\iota} + b(\alpha_i y_i + (1-b_i)\acute{y_\iota}) + c(\alpha_i x_i y_i + (1-\alpha_i) y_i \acute{x_\iota}) + d \tag{12}$$

where quantities with the prime superscript are related to the boundary intersection node points and α_i is calculated from Eq. (13):

$$\alpha_i = \begin{cases} 0 & if\ NP_t \in \Omega_{fluid} \\ 1 & if\ NP_t \in \Omega_{Solid} \end{cases} \tag{13}$$

To find the interpolated values of macroscopic variables such as density at each image points, whenever one of the NPs is not interior, since the velocity or density of boundary intersection point is not known, Eq. (13) is replaced by normal gradient equation at corresponding boundary intersection point as given:

$$\frac{\partial \varphi}{\partial n} = an_x + bn_y + c(xn_y + yn_x) \quad (14)$$

where $\frac{\partial \varphi}{\partial n}$ is the gradient of the general macroscopic variable at the boundary intersection points in the direction normal to the boundary and n is the normal unit vector toward the fluid domain in that direction.

Using Eq. (14), density gradients at boundary intersection points (BI) can be calculated from Eq. (15)

$$\frac{\partial \rho}{\partial n} = an_x + bn_y + c(xn_y + yn_x) = 0 \quad (15)$$

Eq. (14) can be rewritten in a generic form as Eq. (16):

$$\alpha(\alpha_i x_i + (1-\alpha_i)n_{xi} + b(\alpha_i y_i + (1-b_i)n_{yi} c(\alpha_i x_i y_i + (1-\alpha_i)(y_i n_{xi} + x_i n_{yi}) + d \quad (16)$$

where α_i is calculated from Eq. (13).

Finally, the interpolated values of the general macroscopic variables at the IPs, in turn, are extrapolated to the corresponding GPs using Eq. (19). For this purpose, the second-order extrapolation method is applied in case of boundary conditions, whereas for Neumann-type boundary conditions the central difference approximation is used to include the known normal gradient of the macroscopic variable at the boundary into the extrapolation formulation

$$boundrary\ condition: \begin{cases} \delta_{GP} = 2\delta_{BI} - \delta_{IP} \\ \left(\frac{\partial \delta}{\partial n}\right)_{BI} = \frac{\delta_{IP} - \delta_{GP}}{\Delta \varepsilon} \end{cases} \quad (17)$$

Where $\Delta\ell$ denotes the spatial distance between the GP and the related IP. For example, extrapolation of the density along the normal direction guarantees no flow penetration condition across the boundary. Thus, one has $(\partial\rho/\partial n)_{BI} = 0$ and from Eq. (15), it can be concluded that:

$$\rho_{GP} = \rho_{IP} \quad (18)$$

In this stage, f_i^{eq} at the ghost point can be calculated from Eqs (2) by knowing the value of the macroscopic variables at the ghost point, ρ ghost. Nonequilibrium distribution functions f_i^{noneq} and at the ghost point are extrapolated by the procedure similar to that used for density computation. Tiwari[13] noted that, however, this extrapolation method of non-equilibrium parts seems to be only first-order accurate, since $f_i^{noneq} = o(\delta f_i)$ overall accuracy of extrapolating the nonequilibrium part becomes second order $o(\delta^2)$.

Then, equilibrium and non-equilibrium parts of density and internal energy distribution functions are added to achieve the distribution functions at the ghost points.

$$\tilde{f}_{I\,GP} = f_{i\,GP}^{eq} + f_{i\,GP}^{noneq} \quad (19)$$

Finally, boundary condition is satisfied by streaming distribution functions at ghost points into the fluid region.

3. Results and Discussion

3.1. Problem statement

In this study, simulated a laminar flow around a NACA 0012 airfoil, which is characterized by a symmetric profile with 12% thickness to chord length ratio.

NACA airfoils have been extensively used for the validation of numerical schemes, thanks to the availability of experimental data for several different profiles. Flow fields are computed at higher values of Reynolds number, specifically Re = 500 till 100,000, at zero angle of attack. The geometry of the two-dimensional computational domain adopted for the present analysis is illustrated in Figure 3 where C indicates the chord length.

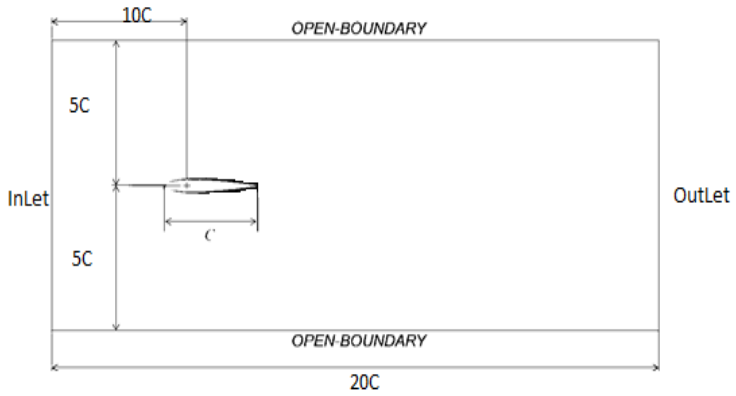

Figure 3: Domain configuration for simulation of fluid flow around NACA 0012 airfoil

3.1.2. Effect of mesh size and domain on the flow variables

Mesh size absolutely depended to length of airfoil chord and domain size. So, by choosing the right size, the results are obtained independently of the mesh. Different mesh sizes are selected in a square domain with the length (L) of the chord 100 unit of lattice. As such, the obtained drag coefficient for different mesh sizes are compared with each other as well as with the experimental solution given in drag results. Aerodynamic coefficients are calculated as follows:

$$C_d = \frac{F_D}{\frac{1}{2}\rho_0 U_0^2 C} \qquad (20)$$

While FD is the drag force, namely the horizontal component of the aerodynamic force acting on the solid body. The effect of mesh size is shown in Table 1, for Re 50,000 and Re=100,000. As depicted in Table 1, it can be seen that as the size of mesh are increased, difference among the results of the simulation decreased. For choosing best size mesh the result has compared with experimental data in reference[14]. Can be seen in this Table, when the mesh size is further increased from 84000 ×1000 to 4000 ×2000, the maximum relative error of 0.1% is seen in drag coefficient. Thus, all the results presented in the following sections are obtained using grid size of 4000 ×1000 in rectangular domain.

Table 1. mesh size effects on the results of drag coefficient at Reynolds $0.5*10^5$ and 10^5

Reynolds	Size	Cd simulation	Cd NASA Report[14]	Error percentage
Re=50,000	1000 ×1000	0.08424	0.052	-62.0%
	2000 ×1000	0.07074		-36.0%
	4000 ×1000	0.051064		1.8%
	4000 ×2000	0.0511054		1.7%
	6000 ×2000	0.051136		1.7%
Re=100,000	1000 ×1000	0.06306	0.037	-70.5%
	2000 ×1000	0.05201		-40.6%
	4000 ×1000	0.03639		1.6%
	4000 ×2000	0.03643		1.5%
	6001 ×2000	0.03647		1.4%

3.2. Result

In this research is discussed the flow fields computed for Re = 500~100,000 in zero angle of attack (α=0) the same computational domain configuration illustrated in Figure 3 is employed, while the chord length is taken to be equal to 100 lattice units, referring to the finest structured refinement level. In this case, for airfoil boundary used ghost flow that has not been done until this time.

Figures 4 show velocity fields for Re = 10000. In order to validate the solution, a comparison between the results obtained by NASA Report [14] Figure 5 reports the values for the drag coefficient as a function of Reynolds number. Note that the two solutions agree with each other very well for the entire range of Reynolds number is investigated.

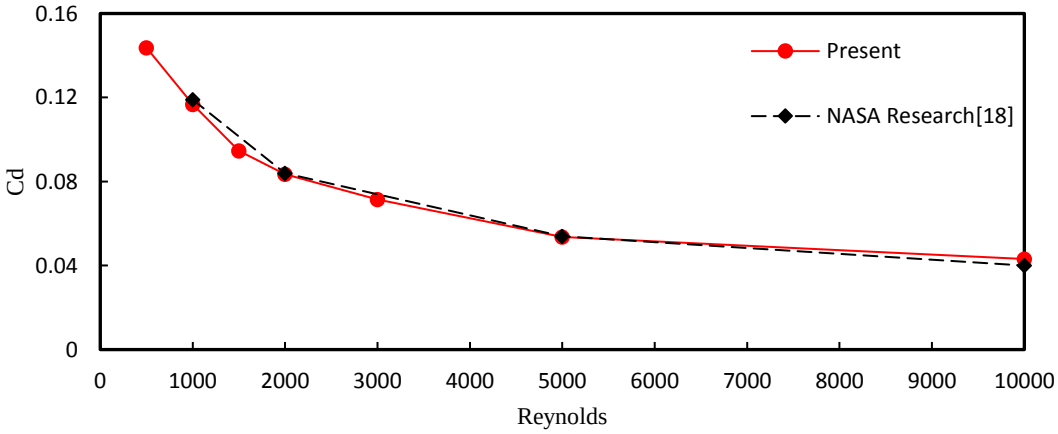

Figure 4: Drag coefficient compared with the Experimental findings of NASA report [14] at a function of the Reynolds in angle of attack = 0

In simulation with this method, the convergence of the results is obtained in a small amount of time. In Fig. 6, the convergence of the drag coefficient for Reynolds 10^5 is shown with an error rate of less than 2%.

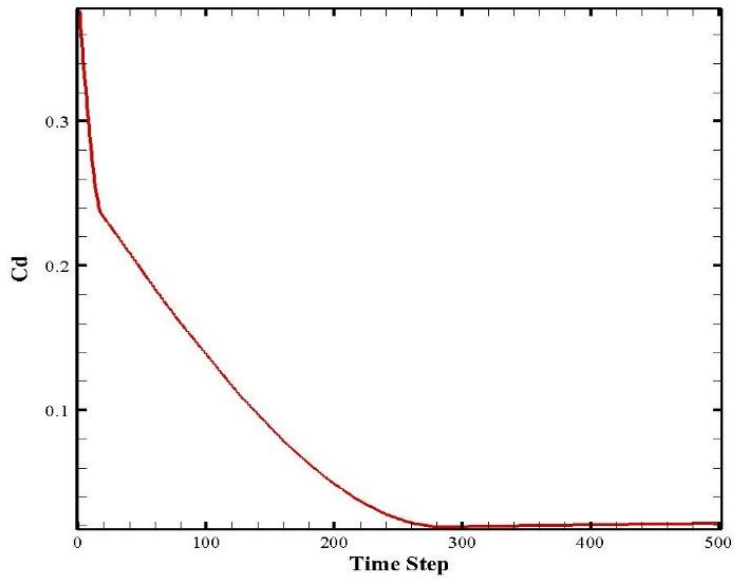

Figure 5: Drag coefficient converging with time step

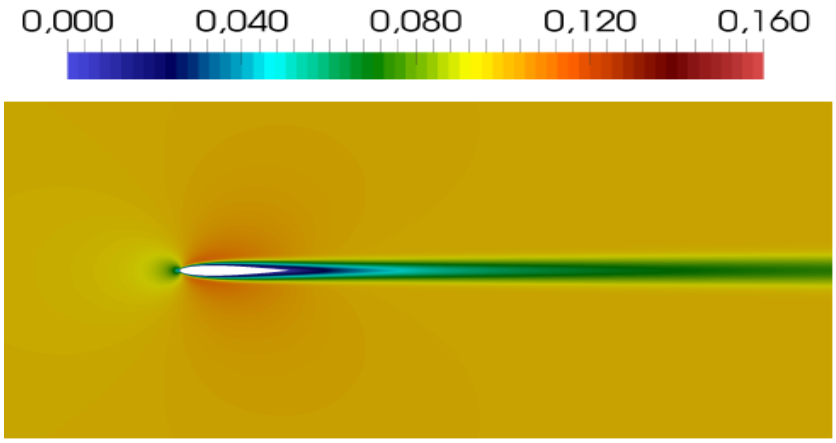

Figure 6: illustrates the instantaneous velocity fields for Re = 100,000 at angle of attack=0.

3. Conclusions

In this paper the NACA 0012 airfoil simulated with ghost flow in lattice Boltzman method were studied, and the effects of drag confection in airfoil was investigated. In the presented method, the inherent feature of the ghost fluid method in computing the gradient of the macroscopic variables normal to the curved boundaries is used to formulate the density and velocity boundary condition. The ghost flow in LBM capability to properly predict the fluid flow behavior of a complex case study, such as that over an airfoil in static stall, has been assessed through this work. Ghost flow in LB model prevents from the need of implementing boundary-fitting procedures for the computation of aerodynamic forces on solid bodies. This property, which is partially lost in traditional lattice Boltzmann approaches, is here fully retained. Further, the method presents high computational efficiency, since the unstructured model is confined to a relatively small portion of the computational domain. Further, the method presents high computational efficiency, since the unstructured model is confined to a relatively small portion of the computational domain. Using ghost flow method in Lattice Boltzmann and observation of results showed the following advantages in this study:

- The new method can capture the details of flow more accurately and more stable than the other schemes, at least in low- Reynolds-number flow.
- The results are in good agreement with the experimental data. With the less grid resolution, and the results converge quickly
- The cost of computing is low compared to similar methods.
- The curve boundary is simulated more accurately and is no considered of the stair-shaped approximation conventionally that used in LBM simulations.

References:

[1] S. Succi, "Lattice Boltzmann 2038," *EPL (Europhysics Lett.*, vol. 109, no. 5, p. 50001, Mar. 2015.

[2] B. Dorschner, S. S. Chikatamarla, and I. V. Karlin, "Transitional flows with the entropic lattice Boltzmann method," *J. Fluid Mech.*, vol. 824, pp. 388–412, Aug. 2017.

[3] S. Di Francesco, C. Biscarini, and P. Manciola, "Numerical simulation of water free-surface flows through a front-tracking lattice Boltzmann approach," *J. Hydroinformatics*, vol. 17, no. 1, pp. 1–6, Jan. 2015.

[4] G. D. Ilio, D. Chiappini, and G. Bella, "A comparison of numerical methods for non-Newtonian fluid flows in a sudden expansion," *Int. J. Mod. Phys. C*, vol. 27, no. 12, p. 1650139, Dec. 2016.

[5] D. Chiappini, "Numerical simulation of natural convection in open-cells metal foams," *Int. J. Heat Mass Transf.*, vol. 117, pp. 527–537, Feb. 2018.

[6] A. Mohamad, *Lattice Boltzmann Method: Fundamentals and Engineering Applications with Computer Codes*. 2011.

[7] X. He and L.-S. Luo, "A priori derivation of the lattice Boltzmann equation," *Phys. Rev. E*, vol. 55, no. 6, pp. R6333–R6336, Jun. 1997.

[8] O. Filippova and D. Hänel, "Grid Refinement for Lattice-BGK Models," *J. Comput. Phys.*, vol. 147, no. 1, pp. 219–228, Nov. 1998.

[9] H. Aono, A. Gupta, D. Qi, and W. Shyy, "The Lattice Boltzmann Method for Flapping Wing Aerodynamics," 2010.

[10] M. Bouzidi, M. Firdaouss, and P. Lallemand, "Momentum transfer of a Boltzmann-lattice fluid with boundaries," *Phys. Fluids*, vol. 13, no. 11, pp. 3452–3459, Nov. 2001.

[11] Z. Guo, C. Zheng, and B. Shi, "An extrapolation method for boundary conditions in lattice Boltzmann method," *Phys. Fluids*, vol. 14, no. 6, pp. 2007–2010, Jun. 2002.

[12] C. T. Orlowski and A. R. Girard, "Modeling and Simulation of Nonlinear Dynamics of Flapping Wing Micro Air Vehicles," *AIAA J.*, vol. 49, no. 5, pp. 969–981, May 2011.

[13] A. Tiwari and S. P. Vanka, "A ghost fluid Lattice Boltzmann method for complex geometries," *Int. J. Numer. Methods Fluids*, vol. 69, no. 2, pp. 481–498, May 2012.

[14] Bragg and M. B., "An experimental study of the aerodynamics of a NACA0012 airfoil with a simulated glaze ice accretion, volume 2," Mar. 1993.